Polymer 51 (2010) 4140–4144

Contents lists available at ScienceDirect

Polymer

journal homepage: www.elsevier.com/locate/polymer

Nanofibers from gas-assisted polymer melt electrospinning

Eduard Zhmayev, Daehwan Cho, Yong Lak Joo*

School of Chemical and Biomolecular Engineering, Cornell University, Ithaca, NY 14853, USA

ARTICLE INFO

Article history:
Received 24 May 2010
Received in revised form
21 June 2010
Accepted 30 June 2010
Available online 7 July 2010

Keywords:
Electrospinning
Polymer melts
Modeling

ABSTRACT

The concept of a gas-assisted polymer melt electrospinning process is presented. This technique allows for reduced quenching of the melt jet in the spinning region, and thus increasing the jet attenuation rate and resulting in production of sub-micron scale fibers. A comprehensive melt electrospinning model was used to analyze the effects of the heated air stream on the polymer jet. It was found that under the investigated conditions in electrospinning of polylactic acid (PLA) melt, air drag produced an additional 10% thinning compared to the un-assisted melt electrospinning process, and the heating provided by the air stream resulted in an additional 20-fold jet thinning.

1. Introduction

Polymer nanofibers, possessing high surface area to mass ratios, have great potential for applications in a wide variety of fields, including high performance filtration, chemical sensing, and biomedical engineering [1–3]. There are several methods currently being researched for micron- and sub-micron-scale fiber forming. Conventional mechanical fiber drawing is one of the most mature methods. Even though high throughputs can be achieved using this method, the resulting fibers are typically ~10–100 μm in diameter [4]. To obtain sub-micron fibers robustly, an additional fiber redraw step, commonly used in optical fiber industry, would have to be employed [5,6]. On the other hand, melt blowing is a promising technique that has been shown to be capable of producing nanofibers in a single stage. However, due to the underlying driving mechanism, the attenuation rate is inherently slow, and thus numerous very small orifices are required to obtain nanofibers with significant throughput [7]. Another approach to produce polymer nanofibers from melts in a single stage is electrospinning [1–3,8–20]. While this process still currently suffers from low throughput, in this report we demonstrate that relatively high attenuation rates can be achieved with some process modifications. These modifications will eventually result in increased throughputs and should position electrospinning as an attractive candidate to address the industrial demand.

In electrospinning, a charged polymer jet is pulled by the action of applied electrostatic force. Initially the jet extends in a straight line and then undergoes whipping motions during the flight from spinneret to collector, where it is finally deposited in the form of a nonwoven fiber mat. Most previous electrospinning studies have involved polymer solutions, which have both economic and environmental drawbacks. Even though the solvents are easily evaporated, the resulting fibers may also be of limited use to medical and bio-related applications. Therefore significant efforts have been dedicated to development of solvent-free electrospinning process with notable recent successes [8–20]. However, significant challenges still exist, particularly in the efforts to reduce the fiber sizes. In this work, we present and analyze an effective method to produce melt electrospun nanofibers.

2. Experimental

The polymer melt electrospinning setup [9], Fig. 1(A), is noticeably more complex than its polymer solution counterpart, particularly due to the need for high temperatures and precise temperature control. Multiple heating zones are used to melt the polymer, prevent it from solidifying near the nozzle, and to convey the high viscosity and low electrical conductivity melts through the spinning region. The enabled melt electrospinning process tends to produce thicker fibers than those from solutions due to the lack of thinning by solvent evaporation. Additionally, the melt jet is typically rapidly quenched by the ambient air, Fig. 1(B), which not only inhibits initial jet attenuation, but also suppresses the whipping motion [8].

* Corresponding author. Tel.: +1 607 255 8591; fax: +1 607 255 9166.
E-mail address: ylj2@cornell.edu (Y.L. Joo).

0032-3861/$ – see front matter © 2010 Elsevier Ltd. All rights reserved.
doi:10.1016/j.polymer.2010.06.058

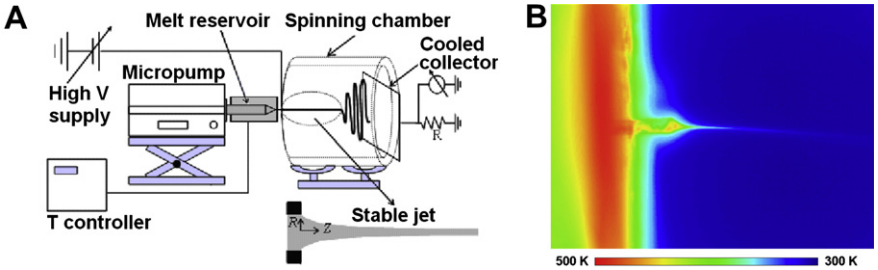

Fig. 1. (A) Schematic of the polymer melt electrospinning setup and (B) a thermal image of polylactic acid melt electrospinning without spinning region heating.

To overcome the aforementioned challenges, additional heating, especially near the nozzle is needed. An infrared (IR) heater is a simple method to heat up the polymer jet in the spinning region. However, the heater footprint is difficult to manage. In multiple experimental trials it was found to be very difficult to precisely control the nozzle temperature (so as not the burn and/or degrade the polymer), while also sufficiently heating the jet in the spinning region. As an alternative solution, we have designed a gas-assisted melt electrospinning (GAME) setup, where a heated gas stream is applied to one of two (or multiple) co-axial jets, as depicted in Fig. 2. This configuration combines conventional melt electrospinning and a gas-jet device in a multi-axial jet format. The gas stream can secure the near-nozzle heating and thus delay solidification of the polymer melt. The high flow rate of the gas can also provide additional drag force to the jet surface, leading to thinner fibers with higher production rate. As a result, due to the additional deformation caused by the heated gas stream, sub-micron scale fibers can be obtained form melt electrospinning. The drastic fiber size reduction is demonstrated in Fig. 3, wherein the average fiber diameter without GAME is 3.5 μm, and with GAME – 0.18 μm. These fibers were spun from polylactic acid (PLA) melt with molecular weight of 186 kDa (purchased from Cargill Dow). The process settings are summarized in Table 1.

It is noteworthy to compare GAME to a related process, electroblowing [21–23], which is also based on a combination of melt blowing and electrospinning concepts. The process was built upon the traditional melt blowing apparatus, with modifications that provided additional deformation due to electric field. However, air drag remained to be the main attenuation driving force and process operation has been successfully demonstrated for only polymer solutions. On the other hand, GAME has been specifically tailored to polymer melts and, as will be shown in the following theoretical analysis, the main attenuation driving force is electric field.

3. Theory and model

In previous publications [9–12], we have presented a comprehensive model for non-isothermal polymer melt electrospinning in the stable jet region. Momentum, mass, and energy conservation equations were derived for a conical jet section and reduced to a 1-D formulation using thin filament approximation. The conservation equations were coupled with diverging electric field and non-isothermal viscoelastic polymer constitutive models (Giesekus and Phan-Thien Tanner). In-flight crystallization equations relevant to a number of fast-crystallizing polymers, *i.e.* Nylon-6 (N6) and polypropylene (PP), have been included. The model approach was validated for amorphous (PLA) and crystallizing (PP, N6) polymers by comparison to experimental jet radius, temperature, and crystallinity profiles from melt electrospinning.

To shed more light on GAME process and the mechanism of the observed increased attenuation rate, and to aid in further process improvement and optimization, the previous melt electrospinning model was modified to account for the drag and thermal effects of the heated air jet. The shear stress due to air drag, τ_D, has been incorporated using the following correlation [4,24]:

$$\tau_D = \frac{1}{2}\rho_{AIR} C_D (V_{AIR} - V)^2 \tag{1}$$

where ρ_{AIR} is the air density, C_D is the skin friction coefficient, V_{AIR} is the axial air velocity, and V is the axial melt jet velocity. It has been assumed that only the stress component axially tangential to the melt jet surface is significant. The skin friction coefficient can be computed using [24–26]:

$$C_D = B\mathrm{Re}_{AIR}^{-0.61} \tag{2}$$

where B is a drag coupling parameter, which typically ranges from 0 to 0.6 [24,27,28], and Re_{AIR} is the air Reynolds number, defined with respect to the melt jet radius, R. Combining equations (1) and (2), and accounting for the stress sign change depending on the relative air and melt jet velocities, the following correlation is obtained:

$$\tau_D = \frac{(V_{AIR} - V)}{|V_{AIR} - V|}\left(\frac{1}{2} B \rho_{AIR}^{0.39} \mu_{AIR}^{0.61} R^{-0.61} |V_{AIR} - V|^{1.39}\right) \tag{3}$$

where μ_{AIR} is the air viscosity. The air drag stress can be non-dimensionalized by the melt reference stress defined in previous publication [9], and incorporated into the previously derived momentum equation:

$$\mathrm{Re}\tilde{V}\frac{d\tilde{V}}{d\tilde{z}} = \frac{1}{\tilde{R}^2}\frac{d\left\{\tilde{R}^2(\tilde{\tau}_{zz} - \tilde{\tau}_{rr})\right\}}{d\tilde{z}} + \frac{1}{Ca\tilde{R}^2}\frac{d\tilde{R}}{d\tilde{z}} + F_E\left\{\tilde{\sigma}\frac{d\tilde{\sigma}}{d\tilde{z}} + \beta_E\tilde{E}_t\frac{d\tilde{E}_t}{d\tilde{z}} + \frac{2\tilde{\sigma}\tilde{E}_t}{\tilde{R}}\right\} - \frac{2\tilde{\tau}_D}{\tilde{R}} \tag{4}$$

where the last term accounts for the air drag, "~" represents dimensionless quantities, defined in [9], Re is the polymer melt jet Reynolds number, τ_{zz} and τ_{rr} are the total axial and radial normal stresses, respectively, Ca is the Capillary number, F_E is the electrostatic force parameter, σ is the surface charge density, β_E is the

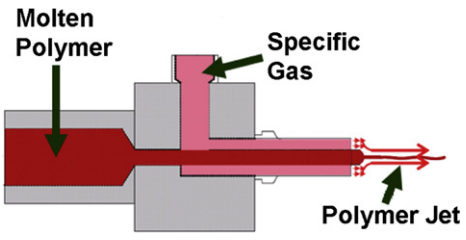

Fig. 2. Schematic of the gas-assisted melt electrospinning nozzle.

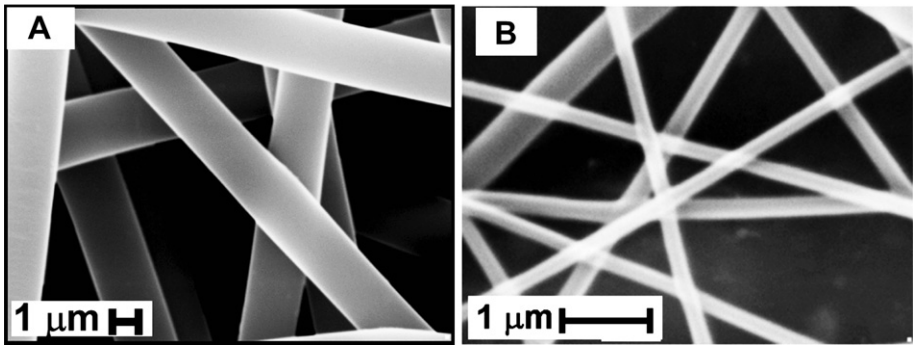

Fig. 3. SEM images of as-melt electrospun PLA fiber mats: (A) without gas-assisted system and (B) with gas-assisted system.

Table 1
PLA melt electrospinning process settings.

Inner (melt) nozzle	4.13×10^{-4} m ID, 7.18×10^{-4} m OD
Outer (air) nozzle	1.194×10^{-3} m ID
Melt flow rate	1.67×10^{-10} m^3/s
Air velocity @ nozzle	300 m/s
Melt temperature @ nozzle	483 K
Air temperature @ nozzle	483 K
Applied potential	2×10^4 V (collector), 0 V (nozzle)
Nozzle to collector distance	0.09 m

dielectric constant ratio, E_t is the component of the electric field tangential to the jet surface, and z is the axial jet coordinate. With the above modifications, the previously developed model can be used to understand GAME process.

For complete details on the model, definitions of the dimensionless numbers and electrostatic terms, and other conservation equations, interested reader is directed to our previous publications [9–12]. The model requires input of a number of PLA thermophysical and rheological properties, but since their values are inconsequential to the present discussion, they are not listed here, and the interested reader is referred to the previous work [9].

4. Results and discussion

Before considering the full complexity of GAME process, some simplified case studies using the modified melt electrospinning model were performed. First, the effect of the stagnant air drag was investigated. As shown in Fig. 4, this drag is negligible in the full range of acceptable B values and typical melt inlet temperatures. This is due to the relatively low jet velocities (V_0/R^2). For example, for the case of $T_{AIR} = 423$ K, the jet velocity ranges from 0.0013 m/s at the spinneret (V_0) to 3 m/s near the collector. In fact, this confirms the negligible air drag assumption used in previous investigations. The learning from this study is that significant air velocities, on the order of 100 m/s, are required to produce the desired additional jet attenuation.

In the next study, various forced air velocities, temperatures, and drag coupling parameters were considered. The forced air velocities and temperatures were taken to be constant and independent of the axial jet position for this illustration. It was observed that the initial attenuation rate remained relatively unchanged by the air drag even at the highest practical air velocities, close to the speed of sound, as shown in Fig. 5. This confirms that the applied electric field is the dominant jet thinning force. Domination of the

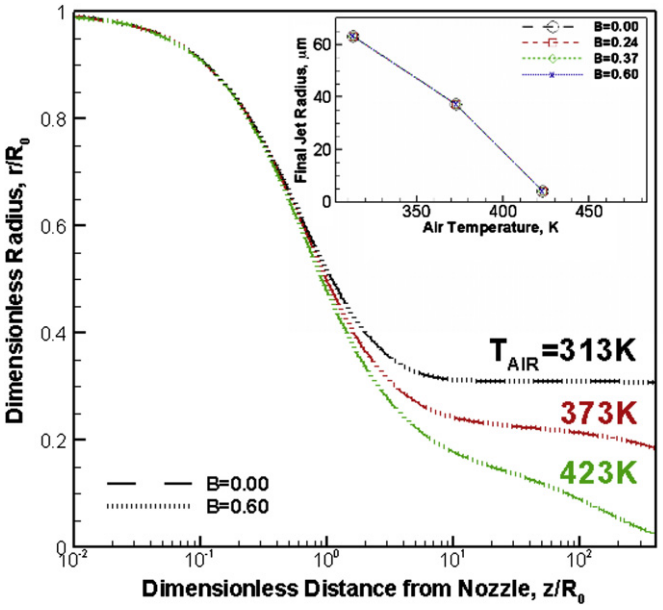

Fig. 4. Effects of the ambient air temperature and air drag on PLA jet radius profiles in melt electrospinning for the case of stagnant air ($V_{AIR} = 0$). Inset shows that final jet sizes are the same for all values of B.

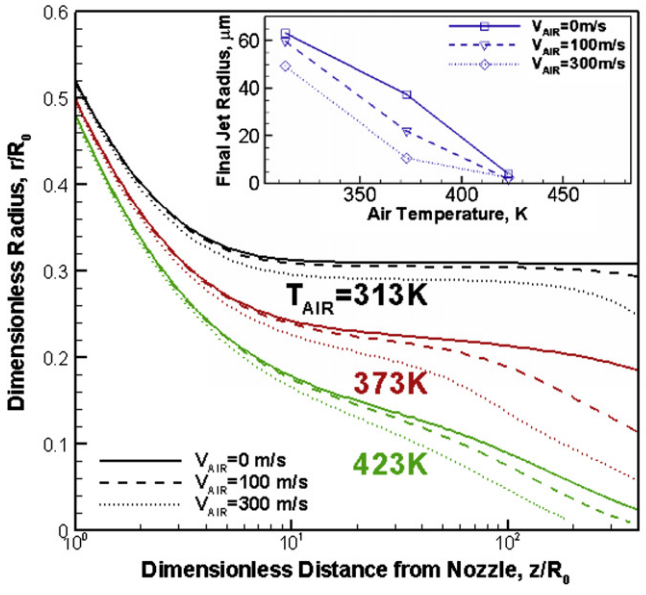

Fig. 5. Effects of the heating air velocity and temperature on jet attenuation in PLA melt electrospinning at $B = 0.6$, and assuming V_{AIR} and T_{AIR} do not change with axial position (z). Inset shows the comparison of the final jet sizes for various air velocities and temperatures.

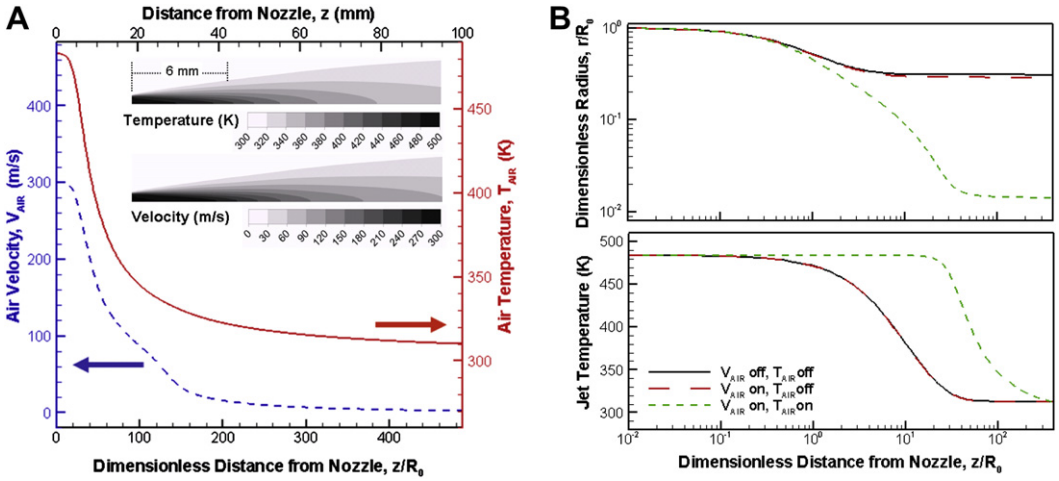

Fig. 6. (A) Heating air temperature and velocity profiles from finite volume analysis (shown in insets), and (B) the corresponding melt electrospinning model results.

electrostatic force is also expected based on previous observations from melt blowing, which exhibited lower attenuation rates. On the other hand, further away from the spinneret, where the electrical driving force decreases due to diverging electric field [9], the air drag effects become apparent and the jets get thinned further than in the stagnant air case. In some of the investigated cases, *e.g.* at $T_{AIR} = 373$ K, as much as 3-fold additional thinning has been observed due to the forced air jet drag. The enhancement is not as pronounced at the extreme temperature conditions due to 1) jet solidification at lower ambient temperatures and 2) high internal stresses developed during rapid initial attenuation at higher temperatures. The effects of varying the value of B (not shown) are similar to varying the air velocity, which is due to the coupling coefficient simply acting as the "efficiency" of the air drag.

Finally, the actual air velocity and temperature profiles were considered. The dynamics of the coupled process are prohibitively complex, so the approach utilized here is similar to that used previously for melt blowing process [29]. The air velocity and temperature profiles were approximated to be independent of the polymer jet dynamics and evaluated numerically using finite volume analysis (with FLUENT™). In the simulation, a high velocity (300 m/s) turbulent air jet at 483 K was injected into the spinning region, initially stagnant air at 300 K, and the steady-state solution was calculated, Fig. 6(A). The resulting axial air velocity and temperature profiles were then used in the modified melt electrospinning model for the calculations of air drag and heat transfer. From the results presented in Fig. 6(B), it is evident that air drag alone results in slight additional jet thinning (final fiber diameter = 57 μm, compared to 63 μm for the base case). However, the additional heating provided by the air jet results in drastically enhanced and prolonged jet attenuation and consequently significantly thinner final jet diameter (2.9 μm). Thus, the heated air jet resulted in a 20-fold decrease in the final fiber diameter, consistently with experimental results presented in Fig. 3. There is a 10-fold difference in the absolute values for the final fiber thicknesses between experimental results and model predictions. As in the previous stable jet models, this is due to omission of the whipping motion of the jet, which will be addressed in future studies. The additional jet thinning due to whipping in the gas-assisted process should be commensurate to the stagnant air cases, since the forced air jet velocity and temperature diminish to the stagnant ambient air quite rapidly, as shown in Fig. 6(A). It should be noted that incorporation of the heated spinning chamber into the GAME setup, as shown in Fig. 1(A) for melt electrospinning case, would inhibit the observed rapid dissipation of air velocity and temperature and therefore produce potentially significant further thinning.

5. Conclusions

To summarize, the gas-assisted polymer melt electrospinning process has been successfully used to produce sub-micron fibers. Modeling analysis was performed, and it was found that at the investigated conditions air drag produced additional 10% thinning compared to the un-assisted melt electrospinning, while the heating provided by the air stream resulted in additional 20-fold thinning. With further process optimization, especially at increased spinning region ambient temperature, even thinner fibers can be produced, and the effects of air drag are expected to become more pronounced.

Acknowledgements

The authors would like to thank the National Science Foundation for funding this work through CAREER Award, grant no. CTS-0448270, and E.I. du Pont de Nemours and Company for funding through Du Pont Young Professor Grant to YLJ.

References

[1] Fong H, Reneker DH. Electrospinning and the formation of nanofibers. In: Salem DR, editor. Structure formation in polymeric fibers, 6. Munich: Hanser Gardner Publications; 2001. p. 225–46.
[2] Dzenis Y. Spinning continuous fibers for nanotechnology. Science 2004;304:1917–9.
[3] Li BD, Xia Y. Electrospinning of nanofibers: reinventing the wheel? Adv Mater 2004;16:1151–70.
[4] Ziabicki A. Fundamentals of fiber formation. New York: Wiley; 1976.
[5] Tong L, Gattass RR, Ashcom JB, He S, Lou J, Shen M, et al. Subwavelength-diameter silica wires for low-loss optical wave guiding. Nature 2003;426:816–9.
[6] Ma L, Matsuura Y. Bragg fiber taper for subwavelength beam generation. J Lightwave Technol 2008;26:3847–52.
[7] Ellison CJ, Phatak A, Giles DW, Macosko CW, Bates FS. Melt blown nanofibers: fiber diameter distributions and onset of fiber breakup. Polymer 2007;48:3306–16.
[8] Zhou H, Green TB, Joo YL. The thermal effects on electrospinning of polylactic acid melts. Polymer 2006;47:7497–505.
[9] Zhmayev E, Zhou H, Joo YL. Modeling of non-isothermal polymer jets in melt electrospinning. J Non-Newt Fluid Mech 2008;153:95–108.

[10] Carroll CP, Zhmayev E, Kalra V, Joo YL. Nanofibers from electrically driven viscoelastic jets: modeling and experiments. Korea-Aust Rheol J 2008;20:153–64.
[11] Zhmayev E, Joo YL. Modeling of crystallizing polymer melts in electrospinning. AIP Conf Proc 2008;1027:9–11.
[12] Zhmayev E, Cho D, Joo YL. Modeling of melt electrospinning for semi-crystalline polymers. Polymer 2010;51:274–90.
[13] Larrondo L, Manley SJ. Electrostatic fiber spinning from polymer melts. I. Experimental observations on fiber formation and properties, II. Examination of the flow field in an electrically driven jet, III. Electrostatic deformation of a pendant drop of polymer melt. J Polym Sci Pol Phys 1981;19:909–40.
[14] Lyons J, Li C, Ko F. Melt-electrospinning part I: processing parameters and geometric properties. Polymer 2004;45:7597–603.
[15] Reneker DH, Yarin AL, Zussman E, Xu H. Electrospinning of nanofibers from polymer solutions and melts. Adv Appl Mech 2007;41:43–195.
[16] Dalton PD, Grafahrend D, Klinkhammer K, Klee D, Moller M. Electrospinning of polymer melts: phenomenological observations. Polymer 2007;48:6823–33.
[17] Dalton PD, Klinkhammer K, Salber J, Klee D, Moller M. Direct in vitro electrospinning with polymer melts. Biomacromolecules 2006;7:686–90.
[18] McCann JT, Marquez M, Xia Y. Melt coaxial electrospinning: a versatile method for the encapsulation of solid materials and fabrication of phase change nanofibers. Nano Lett 2006;6:2868–72.
[19] Ogata N, Yamaguchi S, Shimada N, Lu G, Iwata T, Nakane K, et al. Poly(lactide) nanofibers produced by a melt-electrospinning system with a laser melting device. J Appl Polym Sci 2007;104:1640–5.
[20] Ogata N, Shimada N, Yamaguchi S, Nakane K, Ogihara T. Melt-electrospinning of poly(ethylene terephthalate) and polyalirate. J Appl Polym Sci 2007;105:1127–32.
[21] Armantrout JE, Bryner MA, Spiers CB. Electroblowing fiber spinning process. US Patent No 7,582,247; 2009.
[22] Chu B, Hsaio BS, Fang D. Apparatus for electro-blowing or blowing-assisted electro-spinning technology and process for post treatment of electrospun or electroblown membranes. US Patent Application 2009/0123591; 2009.
[23] Um IC, Fang D, Hsiao BS, Okamoto A, Chu B. Electro-spinning and electro-blowing of hyaluronic acid. Biomacromolecules 2004;5:1428–36.
[24] Joo YL, Sun J, Smith MD, Armstrong RC, Brown RA, Ross RA. 2-D numerical analysis of non-isothermal melt spinning with and without phase transition. J Non-Newt Fluid Mech 2002;102:37–70.
[25] Matsui M. Air drag on a continuous filament in melt spinning. Trans Soc Rheol 1976;20:465–73.
[26] Gould J, Smith FS. Air-drag on synthetic-fibre textile monofilaments and yarns in axial flow at speeds of up to 100 metres per second. J Text Inst 1980;1:38–49.
[27] Denn MM. Correlations for transport coefficients in textile fiber spinning. Ind Eng Chem Res 1996;35:2842–3.
[28] Ziabicki A, Jarecki L, Wasiak A. Dynamic modeling of melt spinning. Comput Theor Polym Sci 1998;8:143–57.
[29] Lewandowski Z, Ziabicki A, Jarecki L. The nonwovens formation in the melt-blown process. Fibers Textiles East Europe 2007;15:77–81.